THE TRANSIENT BEHAVIOR OF CURRENTS AND FORCES IN THE COIL SYSTEM OF THE STELLARATOR W VII ESPECIALLY DURING OPERATIONAL DISTURBANCES

H. Preis

Translation of: "Das transiete Verhalten von Strömen und Kräften im Spulensystem des Stellarators W VII insbesondere bei Betriebsstörungen," Max-Planck-Institut Für Plasmaphysik, Garching Bei München, March 1973, IPP 4/109, 36 pages.

NATIONAL AERONAUTICS AND SPACE ADMINISTRATION
WASHINGTON D.C. 20546 AUGUST 1973

TABLE OF CONTENTS

		PAGE
1.	Introduction	1
2.	Surge power generator installation and operational data	2
3.	Description of the pulse cycle	4
4.	Calculation of the transient currents and forces after a coil short-circuit	12
4.1	Reduction and analysis of the replacement circuit diagram	16
4.2	Evaluation of the network equations	21
4.3	Numerical calculation of the magnetic forces	28

THE TRANSIENT BEHAVIOR OF CURRENTS AND FORCES IN THE COIL SYSTEM OF THE STELLARATOR W VII ESPECIALLY DURING OPERATIONAL DISTURBANCES *

H. Preis

1. Introduction

/ 4**

The toroidal coil system of the Stellarator W VII for producing the main field, consists of 40 uniformly distributed individual coils. In this system, a 40 kA current pulse maintains an average magnetic induction of 40 kG over a pulse duration of 10 seconds. For this order of magnitude of the numerical values, the individual coils are subjected to considerable magnetic forces, which are on the order of more than 100 Mp. A particularly unfavorable coil loading occurs if one coil (or several coils) are suddenly eliminated by means of a short circuit during the operation. In this case, in addition to the centripetal forces acting on the individual coils, there are forces which act in the direction of the axis of the corresponding coil.

The forces mentioned have already been calculated earlier assuming steady state conditions, i.e. all undisturbed coils are completely excited and the short circuited coils have no current [1]. However, the operational state just mentioned can never occur as a consequence of a sudden short circuit.

---

* Max-Planck Institute for Plasma Physics, Garching near Munich, West Germany. This paper was written under a treaty between the Max-Planck Institute for Plasma Physics and the European Atomic Commission on collaboration in plasma physics.

** Numbers in the margin indicate pagination of original foreign text.

In the present investigation, we will make an exact calculation of these forces, in the case of short circuit of one coil. This means that first of all, the transfer functions for the coil currents must be determined, which will be done here while taking into consideration all inductive couplings. In addition, we must consider the fact that a short circuit can occur during any pulse phase. Therefore, there are various ways in which the transient behavior of the currents can be influenced. The calculated current intensities are then used to determine the radial and the axial forces applied to each coil as a function of time. In addition, their maximum values will be determined as a function of the short circuit resistance, which cannot be determined beforehand. /5

2. Surge power generator installation and operational data

The planned Wendelstein VII (W VII) stellarator provides for an energy supply to the coil system by means of a surge power generator [1],[2]. The generator is built in the form of a synchronous generator with two three-phase winding systems which are separated from each other. The energy supply to the W VII magnet is done by means of two three-phase load rectifiers (see Figure 1).

Figure 1 shows only the load circuit of the surge power generator, because it is the only element which is of interest in the calculations which we will carry out. The complete surge power generator installation and its method of operation is given in [1]. The data required for this version was also taken from [1], [2]. These are as follows:

a) Surge-power generator

/6

Useful energy	E	= 1,45 GJ *
Maximum voltage	u_g	= 2 x 2,75 KV
Maximum current	i_g	= 2 x 17,5 KA
Apparent power	N_s	= 167 MVA
Efficiency	N_W	= 155 MW
Frequency	f	= 100 Hz
Rotation rate range	n	= 1650 ÷ 1275 min^{-1}
Total angular momentum	M	= 925 Mpm^2
Times:		
De-excitation time (voltage)	t_e	= 0,4 sec
Flat-top	t_d	= 10 sec
Rise time (standing still up to max. R.P.M.)	t_h	= 25 min
Repetition time	t_w	= 6 min
Braking time	t_b	= 15 min

b) Load rectifier

Maximum direct voltage	u_{ml}	= 3,3 KV
Maximum direct current	i_{max}	= 2 x 22,4 KA

c) Toroidal coil system (see Fig. 5)

Number of main field coils	N	= 40
Diameter of the torus core	d_T	= 4 m
Inner-diameter of the coils	d_i	= 1,1 m
Outer-diameter of the coils	d_a	= 1,9 m
Coil widths	b	= 18,3 cm
Winding number	w	= 25
Internal resistance of the coil at 20° C	R_{i20}	= 0,97 mΩ
Internal resistance of the coil at 40°C	R_{i40}	= 1,06 mΩ
Internal resistance used for the calculation	R_i	= 1 mΩ
Self-inductance of a coil	L_i	= 1,1061 mH
Mutual inductances (see Table 1)		

* Translator's Note: Commas represent decimal points.

d) Helix

Number of helical windings	$n_H = 4 \times 24 = 96$
Inclination	$h = d_T/2,5$
Resistance	$R_H = 20\ m\Omega$
Inductance	$L_H = 10\ mH$

/7

e) Operational data

Magnetic field along the torus core	$B = 40\ KG$
Nominal current (for 10 sec flat-top)	$I_N = 40\ KA$
Total resistance ($R_g = R_H + 40 \cdot R_l$)	$R_g = 60\ m\Omega$
Total inductivity ($L_g = L_H + \sum_{l=1}^{40} \sum_{j=1}^{40} L_{ij}$)	$L_g = 180\ mH$

Voltage at the magnet $u_{m(t)}$ (see Fig. 2)

3. Description of the pulse cycle

The mesh differential equations which apply for Figure 1 can be used to describe the magnetic current $i_{(t)}$.

$$L_g\, i'_{(t)} + R_g\, i_{(t)} = u_{m(t)} \qquad (1)$$

or

$$\frac{d i_{(t)}}{dt} + \delta \cdot i_{(t)} = \frac{u_{m(t)}}{L_g} \qquad (2)$$

with

$$\delta = \frac{R_g}{L_g} \qquad (3)$$

The general solution is given by:

$$i_{(t)} = e^{-\delta (t-t_o)} \left[i_{(t_o)} + \frac{1}{L_g} \int_{t_o}^{t} u_{m(x)}\, e^{\delta (x-t_o)}\, dx \right] \qquad (4)$$

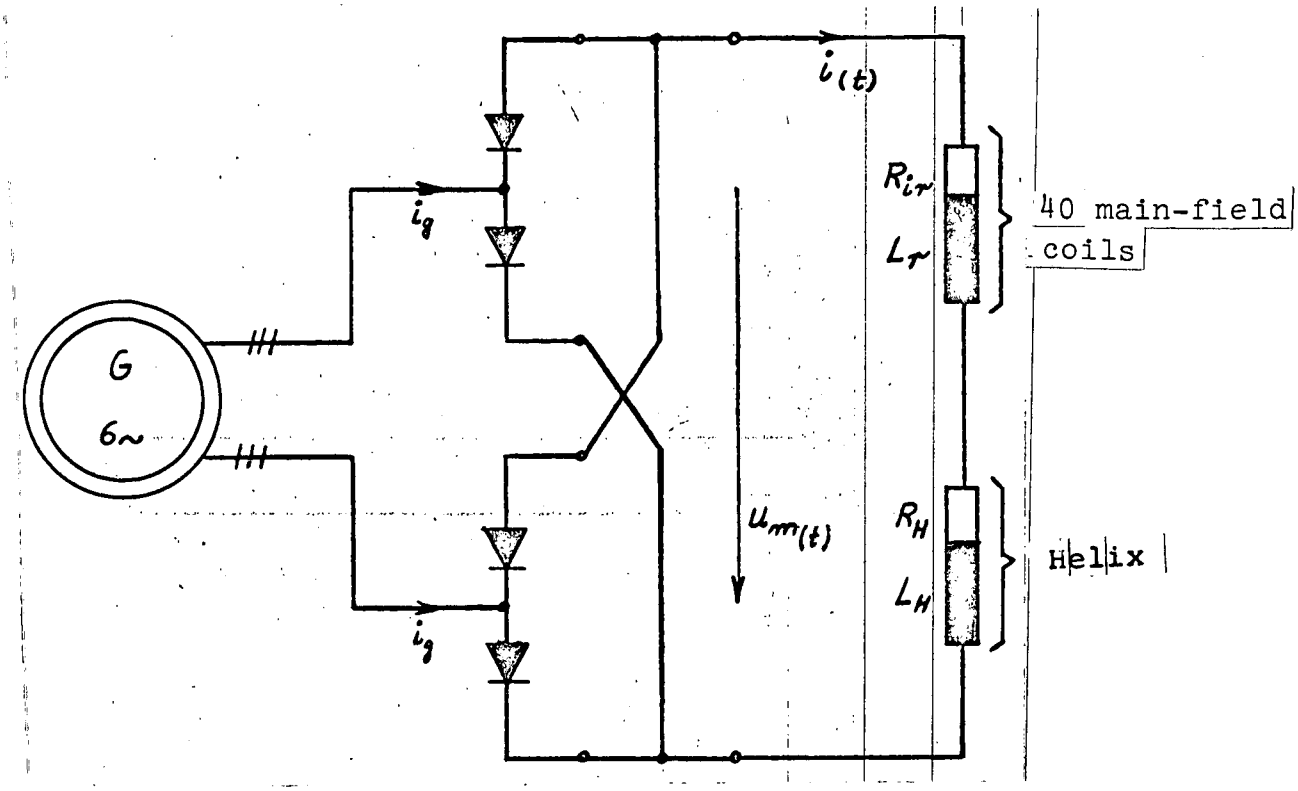

Figure 1. Load circuit of the surge power generator.

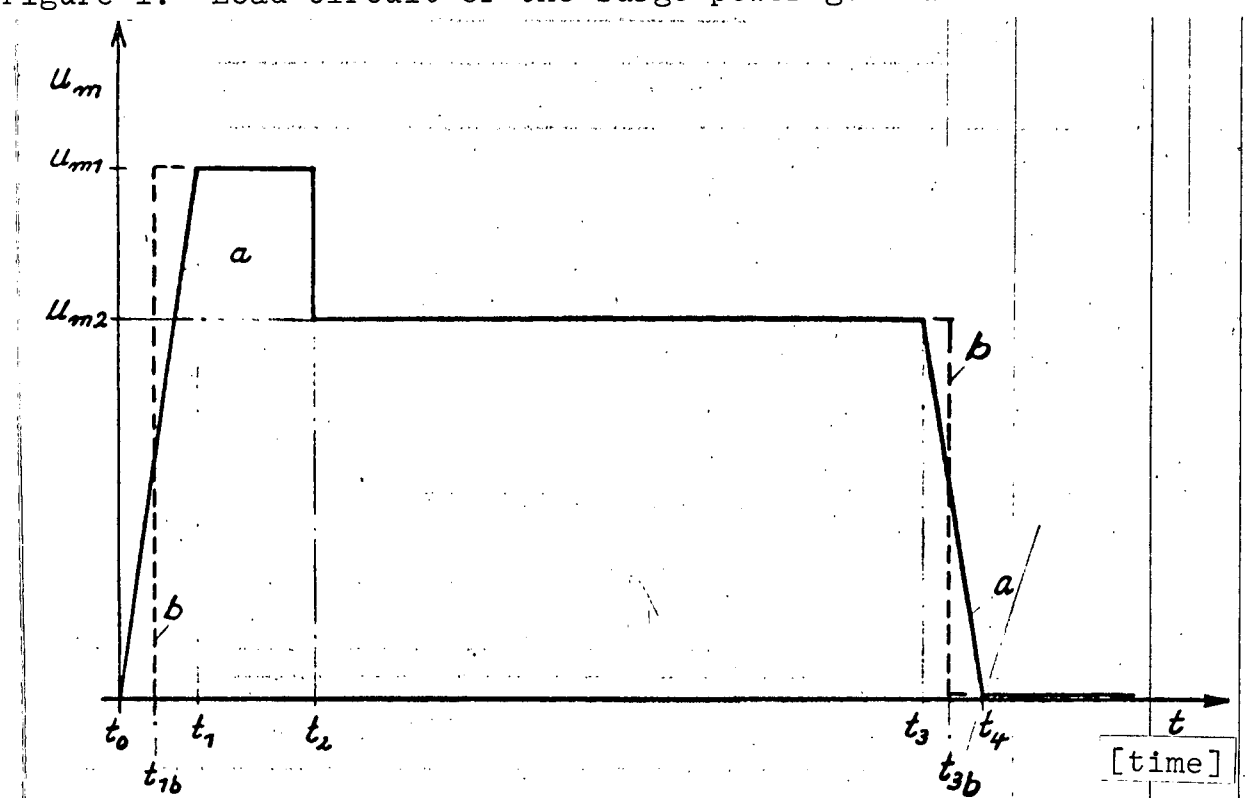

Figure 2. Voltage variation $u_{m(t)}$ at the magnet. Curve a is the real and Curve b is the idealized variation.

Before we specialize this equation for the individual phases of the pulse cycle, we must describe the time behavior of the driving voltage $u_{m(t)}$ applied to the coil system. We mean the voltage which occurs across a load rectifier switched in after the surge-power generator. During a pulse cycle, it has the following (Figure 2) variation, which can be reproduced by means of a voltage control or a current control [3] in the excitation circuit of the surge generator.

/ 8

Of course it is not possible to influence the magnet voltage $u_{m(t)}$ with the excitation surface without any inertia, because no infinitely fast current changes are possible in the excitation circuit. This means that $u_{m(t)}$ also cannot carry out any discontinuous changes during the initial excitation or de-excitation. The operational data given in Section 2 show that the de-excitation time referred to the voltages (from $U_{m2} = 2.4$ KV to $U_{m2} = 0$) is equal to $t_e = t_4 - t3 = 0.4$ sec. This corresponds to a possible voltage change of

$$a = \frac{\Delta u}{\Delta t} = \frac{2{,}4 \text{ KV}}{0{,}4 \text{ sec}} = 6 \frac{\text{KV}}{\text{sec}} \qquad (5)$$

/9

Taking (5) into account, we find the voltage variation (curve a) given in Figure 2, which is as follows:

$$u_{m(t)} = \begin{cases} at & \text{for } t_o \leq t \leq t_1, \text{ 1. Range} \\ u_{m1} & \text{for } t_1 \leq t \leq t_2, \text{ 2. Range} \\ u_{m2} & \text{for } t_2 \leq t \leq t_3, \text{ 3. Range} \\ u_{m2} - a(t-t_3) & \text{for } t_3 \leq t \leq t_4, \text{ 4. Range} \\ 0 & \text{for } t_4 \leq t \leq t_E, \text{ 5. Range} \end{cases} \qquad (6)$$

It is possible to solve equation (4) in parts, using this expression. We find the following for the individual phases:

First range (initial excitation phase)

$$i_{(t)} = e^{-\delta \cdot t}\left[i_{(o)} + \frac{a}{L_g}\int_o^t x e^{\delta x} \cdot dx \right]$$

or with the initial value $i_{(o)} = 0$

$$i_{(t)} = \frac{a}{L_g \delta^2}\left[\delta \cdot t - 1 + e^{-\delta \cdot t}\right] \quad \text{für } 0 \leq t \leq t_1 \qquad (7)$$

where

$$t_1 = \frac{u_{m1}}{a} = \frac{3{,}3\ \text{KV}}{6\ \text{KV sec}^{-1}} = 0{,}55\ \text{sec} \qquad (8)$$

in addition

$$i(t_1) = 4.7472\ \text{KA} \qquad (9)$$

is the initial value for the next region.

/ 10

Second range (initial excitation phase)

$$i_{(t)} = e^{-\delta(t-t_1)}\left[i_{(t_1)} + \frac{u_{m1}}{L_g}\int_{t_1}^t e^{\delta(x-t_1)}\, dx \right]$$

or

$$i_{(t)} = \frac{u_{m1}}{R_g} + \left(i_{(t_1)} - \frac{u_{m1}}{R_g}\right)e^{-\delta \cdot (t-t_1)} \quad \text{für } t_1 \leq t \leq t_2 \qquad (10)$$

using equation (10) and the condition

$$i_{(t2)} = I_N = 40\ \text{KA (Nominal current)}$$

The initial excitation time is calculated as:

$$t_2 = t_1 - \frac{1}{\delta} \cdot \ln \frac{i(t_2) - \frac{U_{m1}}{R_g}}{i(t_1) - \frac{U_{m1}}{R_g}} = 4{,}18 \text{ sec} \qquad (11)$$

Third range (flat-top phase)

$$i_{(t)} = e^{-\delta \cdot (t-t_2)} \left[i_{(t_2)} + \frac{u_{m2}}{L_g} \int_{t_2}^{t} e^{\delta \cdot (x-t_2)} \, dx \right]$$

$$\text{or } i_{(t)} = \frac{u_{m2}}{R_g} + \left(i_{(t_2)} - \frac{u_{m2}}{R_g}\right) e^{-\delta \cdot (t-t_2)} \text{ for } t_2 \leq t \leq t_3 \qquad (12)^*$$

The previous equation immediately shows that

$$i_{(t)} = \frac{u_{m2}}{R_g} = \text{const.} \qquad (13)$$

if, at the beginning of this range, there is a voltage reduction to

$$u_{m2} = i_{(t2)} \cdot R_g = 40 \text{ KA} \cdot 60 \text{m}\Omega = 2{,}4 \text{ KV} \qquad (14)$$

/ 11

This provides a transition to the flat-top phase without any oscillations, for optimally fast initial excitation.

Since we have assumed a pulse ceiling of

$$t_i = 10 \text{ sec}$$

we find

$$t_3 = t_2 + t_i = 14.18 \text{ sec} \qquad (15)$$

Fourth range excitation

$$i_{(t)} = e^{-\delta \cdot (t-t_3)} \left[i_{(t_3)} + \frac{1}{L_g} \int_{t_3}^{t} (u_{m2} - ax) e^{\delta \cdot (x-t_3)} \, dx \right]$$

---

* Here a voltage drop from u_{m1} to u_{m2} has been assumed because the real discharge time is smaller than 0.1 sec.

or

$$i_{(t)} = \frac{u_{m2}}{R_g} - \frac{a}{\delta^2 L_g}\left[e^{-\delta(t-t_3)} + \delta(t-t_3) + 1\right] \quad \text{for } t_3 \leq t \leq t_4 \tag{16}$$

where

$$t_4 = t_3 + \frac{u_{m2}}{a} = 14{,}58 \text{ sec} \tag{17}$$

In addition

$$i_{(t_4)} = 37.448 \text{ KA} \tag{18}$$

is the initial value for the last range.

Fifth range (de-excitation phase)

$$i_{(t)} = i_{(t_4)} e^{-\delta(t-t_4)} \quad \text{for } t_4 \leq t \leq t_E \tag{19}$$

Using the equations (7) to (19), we have given a complete description of the transient behavior of the magnet current $i_{(t)}$. It is shown by the curve given in Figure 3. / 12

For comparison purposes, Figure 4 gives the course of $i_{(t)}$ if $u_{m(t)}$ is approximated by means of a jump function according to curve b of Figure 2. In this case, $i_{(t)}$ follows the following analytical representation.

$$i_{b(t)} = \begin{cases} 0 & \text{for } 0 \leq t \leq t_{1b} \\ \frac{u_{m1}}{R_g}\left(1 - e^{-\delta(t-t_{1b})}\right) & \text{for } t_{1b} \leq t \leq t_2 \\ \frac{u_{m2}}{R_g} & \text{for } t_2 \leq t \leq t_{3b} \\ i_{(t_{3b})} e^{-\delta(t-t_{3b})} & \text{for } t_{3b} \leq t \leq t_E \end{cases} \tag{20}$$

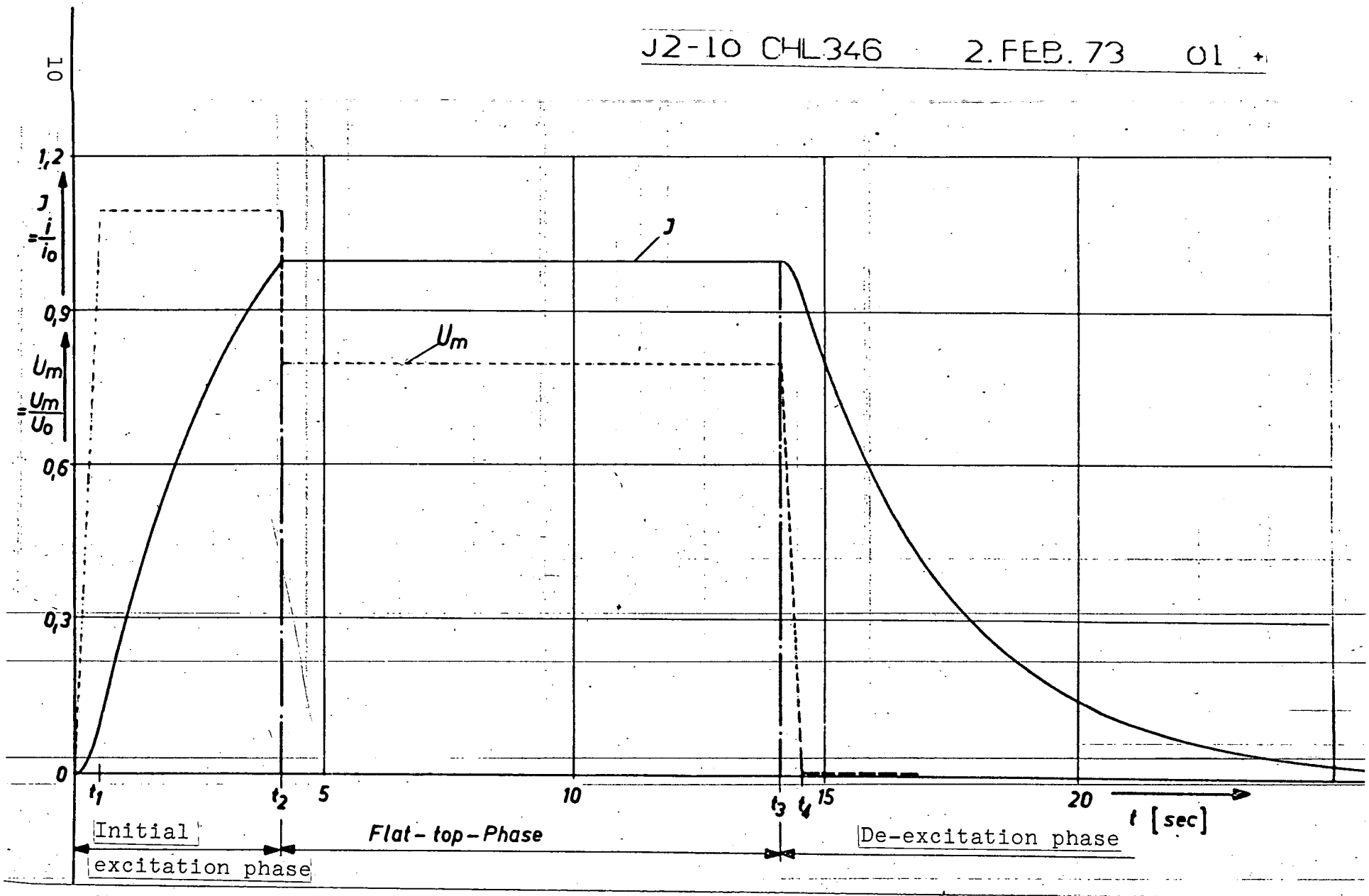

Figure 3. Pulse cycle of the coil currents $i_{(t)}$ and the magnet voltage $u_{m(t)}$.

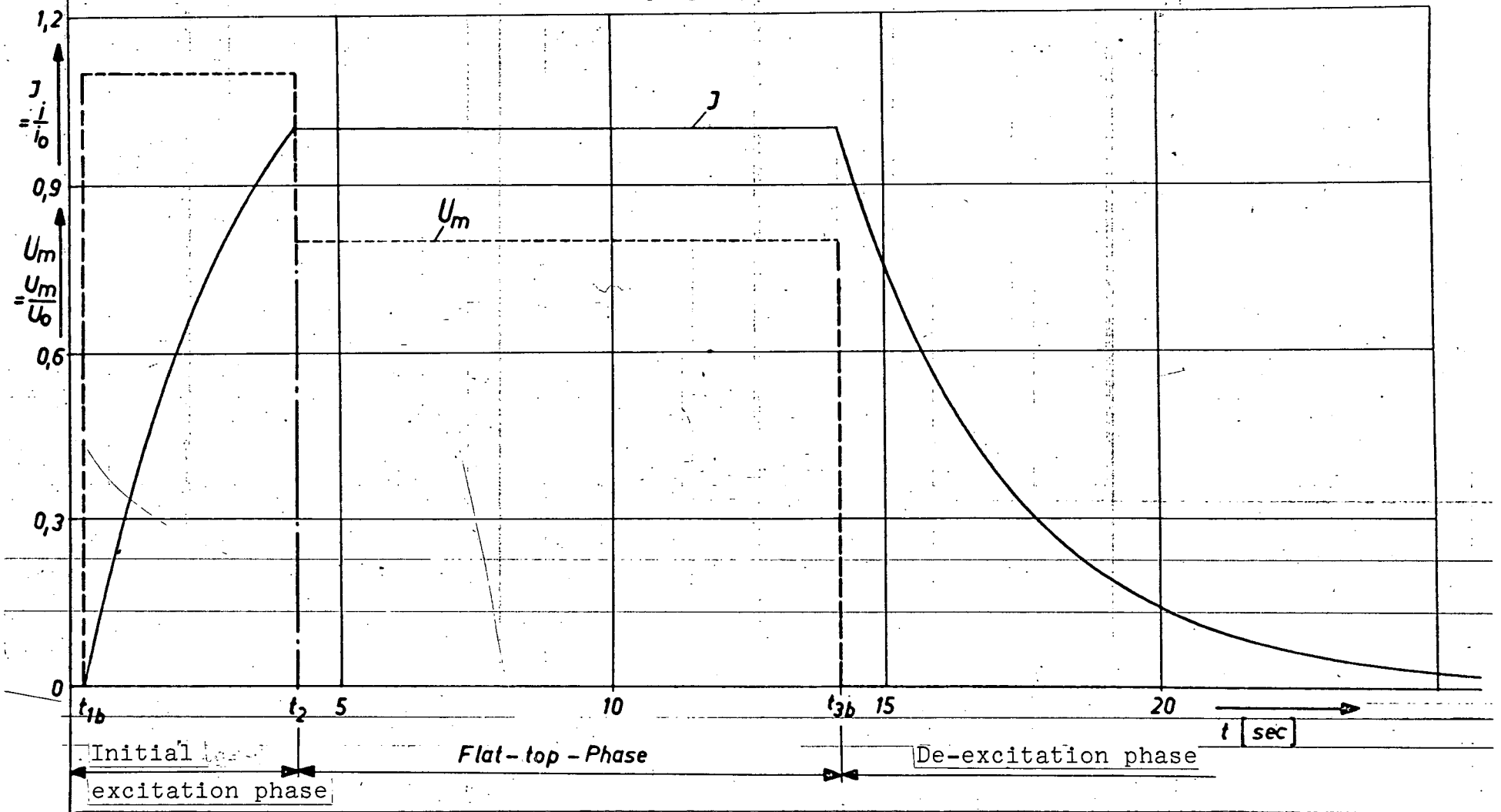

Figure 4. Idealized cycle of the coil currents $i_{b(t)}$ and the magnet voltage $u_{m(t)}$.

which holds for the new interval division

$$t_{1b} = \frac{t_1}{2}$$

$$t_{2b} = t_2$$

$$t_{3b} = t_3 + \frac{t_4 - t_3}{2}$$

A comparison of the two functions $i_{(t)}$ and $i_{b(t)}$ resulted in such small deviations, with the exception of the beginning of the pulse, that the relationships (20) were used in order to simplify the computation process.

/15

4. Calculation of the transient currents and forces after a coil short circuit.

In order to produce a closed magnet field configuration, the Stellarator W VII consists of N = 40 individual coils arranged in a toroid (Figure 5). They are operated in series and therefore they all carry the same current in the same direction around the torus tube. This again leads to a symmetric magnetic field in the toroid, i.e. magnetic field lines are closed concentric circles around the symmetry plane of the torus except for slight bulges at the coil gaps. Superimposed on the field just described, there is another field which is due to the current of a winding which has a spiral shape around the torus tube. However, in this paper we will not consider the influence of the helical winding which surrounds the main field coils. We would only like to mention that it is switched in series with the first field (Figure 6).

B

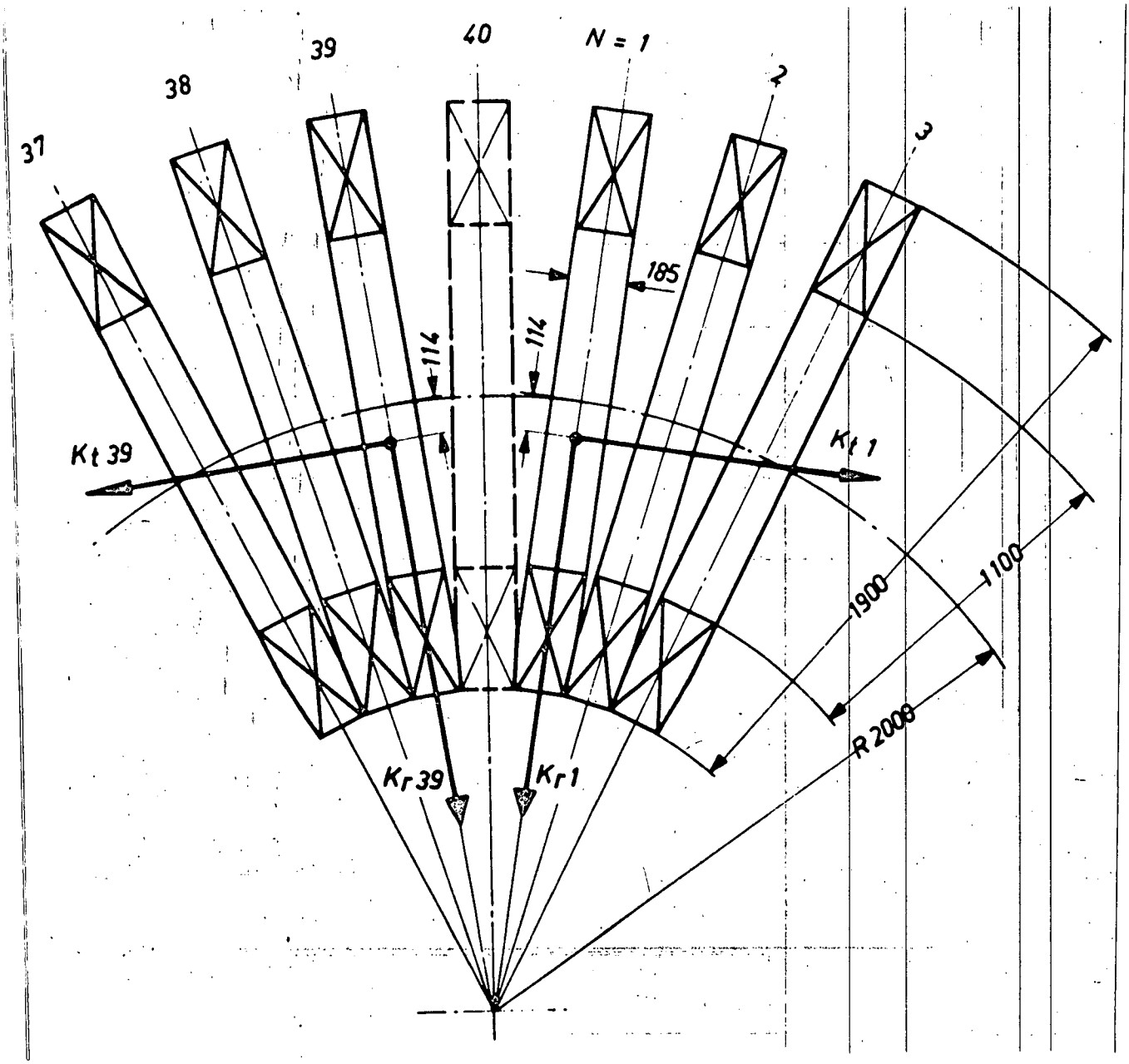

Figure 5. Segment from the toroidal coil arrangement with the resulting forces at Coils 1 and 39, after Coil 40 has been short circuited.

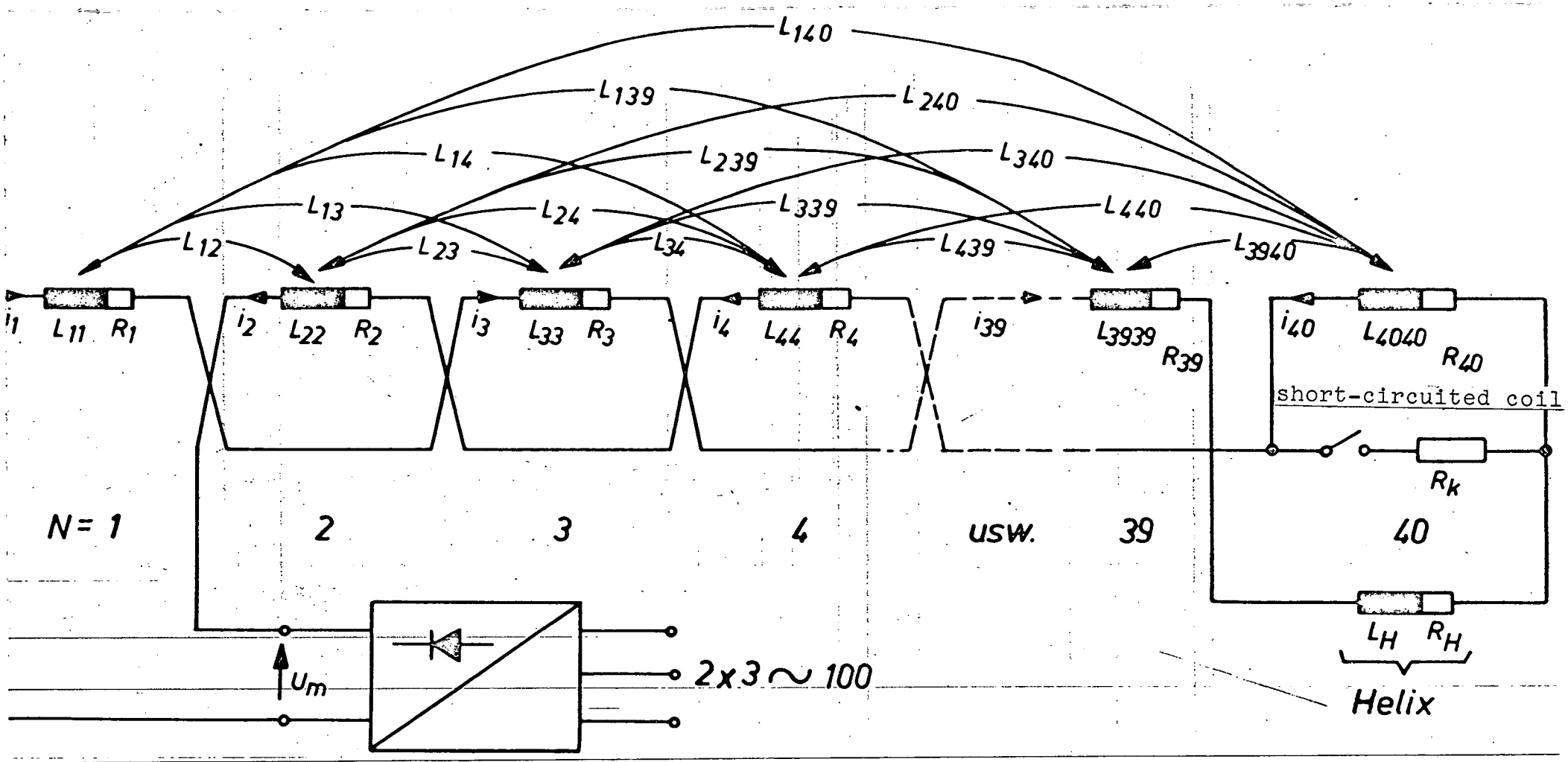

Figure 6. Replacement circuit diagram of the W VII magnets.

Starting with the field line variation described above, for the main field, we can immediately make a statement regarding the effective Lorentz forces which act on the coil system.

$$\vec{K} \sim \vec{G} \times \vec{B} \qquad (21)$$

For expediency, the magnetic induction vector $\vec{B}$ is decomposed into a radial component B_r and a component B_t which is tangential to the torus core. Both are perpendicular to the current density vector $\vec{G}$ at any radial winding cross section, so that according to equation (21) there is a force K_t tangential to the torus core and a radial force K_r, which are applied to each coil. For undisturbed operational conditions, (i.e. equal current intensity in all coils) B_r is directed inwards over 1/2 of the coil width and outwards over the other half, because of the symmetrical design of the installation.

/17

In addition, the magnitudes are the same at equivalent positions. Therefore, according to (21) and by summing all infinitesimal cross-section forces, the resulting tangential force K_t vanishes. In contrast to this, all coils are subjected to an equally large resulting radial force K_r. More specifically, these are centripetal forces, because if the current density $\vec{G}$ is locally constant over the cross-section of the coils, the magnetic induction B_t decreases as the distance to the center of the system is increased. This means that the resulting radial forces directed to the outside and acting on the coil elements along the outer torus edge are smaller than those which are directed inwards and which are applied to the coil elements along the inner torus edge.

If there is a sudden disturbance in the operation, caused by a short circuit or similar circumstances, the short circuited coil prematurely begins to discharge through the short circuit

resistance. This results in various current intensities in the individual coils, which then produce an asymmetric magnet field, in particular B_r. According to (21), a B_r which has an asymmetric distribution over the coil width results in a force K_t which is applied to all the coils, in addition to the radial force K_r discussed above. The only exception to this is the short circuited coil itself because in it B_r will be symmetric just like before, which again means $K_t = 0$. On the other hand, the largest tangential force K_t is applied to the coils adjacent to the disturbed coil. This tangential force decreases rapidly for the coils as their distance to the disturbed coil increases.

The following investigation is restricted to the case of a short-circuited coil.

/ 18

In order to calculate the transient forces during a premature discharge of a coil, the transient behavior of the coil current $i_{N(t)}$ (N = 1 to 40) is of particular significance. It must be calculated here considering all the inductive couplings. The required coupling coefficients (self-inductance and mutual inductance) of the system were already given earlier in [1]. They are calculated on the basis of [4]. This means that a replacement circuit diagram according to Figure 6 can be used for the calculations. It is assumed that at the time $t = t_k$ there is a short circuit through the coil N = 40. This assumption does not restrict the generality, because we are dealing with a symmetric coil arrangement (Figure 5).

4.1 Reduction and analysis of the replacement circuit diagram / 20

In order to analyze the replacement circuit diagram shown in Figure 6, we would like to carry out an obvious simplification.

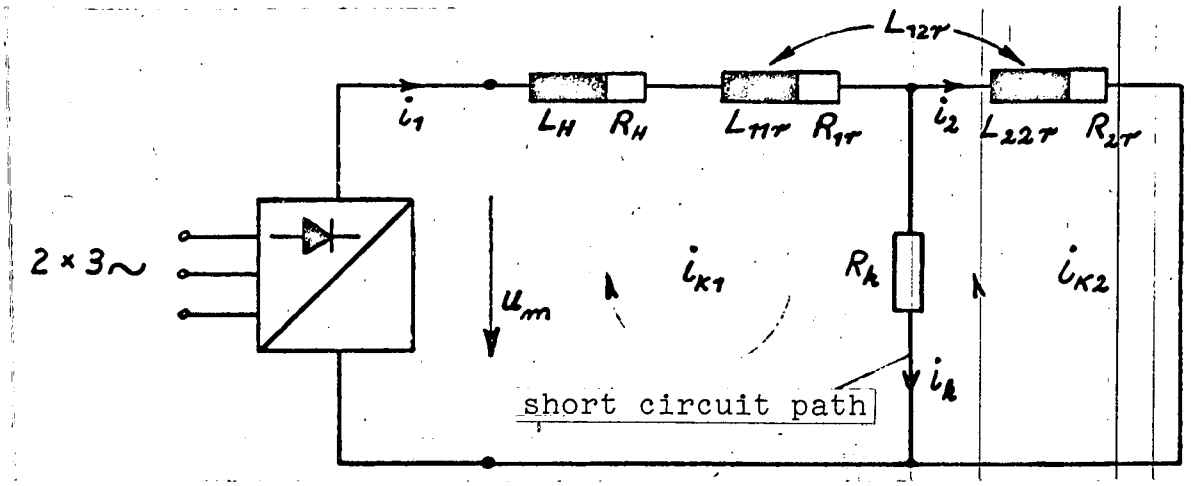

Figure 7. Reduced replacement circuit for the W VII magnet.

All circuit elements which are in series can be collected, without losing the influence of the overall inductive couplings. A circuit shown in Figure 7 then remains.

This means that if, out of a total of n-coils, the last n-m are short-circuited, we have the following for the resulting replacement elements:

Resistance of all undamaged coils

$$R_{1r} = \sum_{i=1}^{m} R_i \qquad (22)$$

Resistance of all short-circuited coils

$$R_{2r} = \sum_{i=m+1}^{n} R_i \qquad (23)$$

Self-inductance of all undamaged coils

$$L_{11r} = \sum_{i=1}^{m} \sum_{j=1}^{m} L_{ij} \qquad (24)$$

/ 21

Self-inductance of all short-circuited coils

$$L_{22r} = \sum_{i=m+1}^{n} \sum_{j=m+1}^{n} L_{ij} \qquad (25)$$

Mutual inductance between the short-circuited and undamaged coils

$$L_{12r} = \sum_{i=1}^{m} \sum_{j=m+1}^{n} L_{ij} \qquad (26)$$

If we specialize those equations obtained for the case under consideration, that is, n = 40 and m = 39, we find the following values using the numerical values given in [1], [2].

Resistances R_i = 1 m Ω for i = 1 to 40

Self-inductances L_{ii} = 1.1061 mH for i = 1 to 40

Mutual inductances

j	$L_{i,i+j}$ [mHenry]
1	0,64602 *
2	0,31332
3	0,17843
4	0,11198
5	0,07682
6	0,05548
7	0,04114
8	0,03112
9	0,02392
10	0,01861
11	0,01464
12	0,01162
13	0,00930
14	0,00751
15	0,00612
16	0,00505
17	0,00425
18	0,00369
19	0,00335
20	0,00324

* Translator's Note: Commas represent decimal points.

The following results are obtained

/22

$$R_{1r} = \sum_{1}^{39} R_i = 39 \text{ m}\Omega$$

$$R_{2r} = \sum_{40}^{40} R_i = 1 \text{ m}\Omega$$

$$L_{11r} = \sum_{1}^{39} \sum_{1}^{39} L_{ij} = 162{,}002 \text{ mH}$$

$$L_{22r} = \sum_{40}^{40} \sum_{40}^{40} L_{ij} = 1{,}1061 \text{ mH}$$

$$L_{12r} = \sum_{40}^{40} \sum_{1}^{39} L_{ij} = 3{,}1280 \text{ mH}$$

After preparing the switching elements, we can now carry out the mesh analysis of the reduced circuit [5, 6]. According to it, the branch currents

$$(i) = (H)\,(i_k) \tag{27}$$

are related to the arbitrarily selectable circuit currents (i_k) by means of a structural matrix (H). * Using the transposed structural matrix $(H)^T$, we can also formulate the following two independent voltage paths, for the circuit under discussion (Figure 7).

$$0 = (H)^T(u) \tag{28}$$

where the branch voltages

$$(u) = (u_R) + (u_L) + (u_o) \tag{29}$$

consist of the individual voltage drops

* Letters in parentheses are symbolic notations for matrices and vectors, respectively.

$$(u_R) = (R_d)\ (i) \tag{30}$$

/ 23

$$(u_L) = \frac{d}{dt}\left[(L_d)\cdot(i)\right] = (L_d)\,(i') \tag{31}$$

and the source voltages (u_o). By substituting equation (27) into (31), we are led to the following differential equation system of the first order:

$$(i_k') = -\,(L)^{-1}(R)\,(i_k) - (L)^{-1}(H)^T(u_o) \tag{32}$$

with

$$(L) = (H)^T(L_d)\,(H) \tag{33}$$

$$(R) = (H)^T(R_d)\,(H) \tag{34}$$

$$(H) = \begin{bmatrix} 1 & 0 \\ 0 & 1 \\ 1 & -1 \end{bmatrix} \quad ; \quad (H)^T = \begin{bmatrix} 1 & 0 & 1 \\ 0 & 1 & -1 \end{bmatrix} \tag{35}$$

$$(L_d) = \begin{bmatrix} L_{11r} & L_{12r} & 0 \\ L_{21r} & L_{22r} & 0 \\ 0 & 0 & 0 \end{bmatrix} \quad ; \quad L_{12r} = L_{21r} \tag{36}$$

$$(R_d) = \begin{bmatrix} R_{1r} & 0 & 0 \\ 0 & R_{2r} & 0 \\ 0 & 0 & R_k \end{bmatrix} \tag{37}$$

$$(u_o) = \begin{bmatrix} u_m \\ 0 \\ 0 \end{bmatrix} \tag{38}$$

In order to give a unique solution for this differential equation system (32), we must specify the initial conditions / 24

$$(i_k(t_k)) = \begin{bmatrix} i_{k1}(t_k) \\ i_{k2}(t_k) \end{bmatrix} \tag{39}$$

These are the current intensities of the circuit currents at the time t_k, at the beginning of the short circuit. These can easily be calculated from the equations for undisturbed operational conditions (see Section 3).

As a numerical solution method for equation (32), we will use the predictor-corrector method given by Hamming [7]. It has been written as a Fortran routine with the name "Netzwerke 2." Details are given in [6].

4.2 Evaluation of the network equations.

We will now evaluate the derived network equations. Of course this must be done in parts within the individual adjacent ranges of validity, i.e. the equations for undisturbed operation apply for $t \leq t_k$ whereas equation (32) applies for $t \geq t_k$. The time t_k is the time at which a possible short circuit occurs. Of course, this time could be within any pulse phase. Because of the fact that the discharge processes will certainly differ, we must distinguish between a short circuit during an initial excitation phase and during the flat-top phase. Both cases must be analyzed. We will not decide whether or not the de-excitation of the surge generator and therefore the de-excitation of the total system (the magnet voltage u_m is reduced to zero) must be carried out immediately after a short circuit. This is certainly a question which must be discussed in detail. If we were to decide for a premature de-excitation because it has the advantage of a lower and shorter loading of the coils by the

tangential forces K_t, then a surveillance installation would be required for each coil, which would signal the disturbance and would begin the de-excitation immediately. It is likely that such an installation will be required anyway because of the possible other types of disturbances (for example, sudden interruption in the current circuit). Accordingly, we must distinguish among the following cases in the evaluation. /25

a) Coil short circuit during the initial excitation phase with immediate initiation of the generator de-excitation.

According to Figure 3, the initial excitation range extends from t_o = 0 sec to t_2 = 4.18 sec. Within these limits, that is, at t_k = 4 sec (just before the nominal current I_N is reached) we will simulate a short circuit.

At the point t_k we have

$$i_{(t)} < I_N = 40 \text{ KA}$$

$$i'_{(t)} \neq 0$$

$$u_{m(t)} = \begin{cases} \text{corresponding to Eq. (6)} & \text{for } t \leq t_k \\ u_{m1} - a(t-t_k) & \text{for } t_k \leq t \leq t_{k1} \\ 0 & \text{for } t_{k1} \leq t \leq t_E \end{cases}$$

$$R_k = 1 \text{ m}\Omega$$

Here R_k is the resistance of the short circuit path. Its influence will be studied later on more accurately. First we will assume the value given above. The transition functions $i_{(t)}$ which are obtained for these side conditions are shown in Figure 8 by curves. Similar curves are shown in Figure 9 for the ideal short circuit (R_k=0).

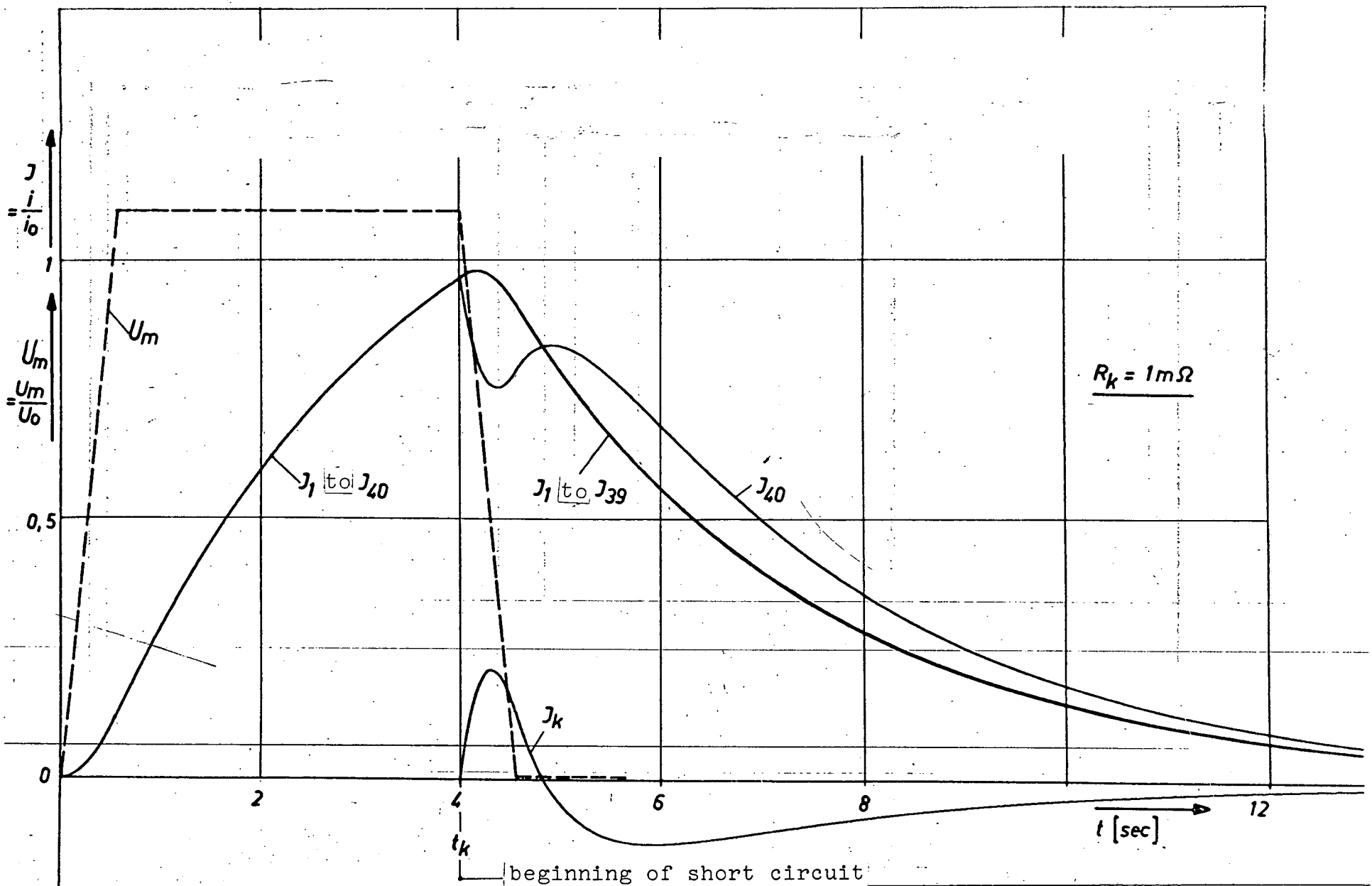

Figure 8. Coil currents $i_{(t)}$ and magnet voltage $u_{m(t)}$ for a coil short circuit in the initial excitation phase with immediate generator de-excitation.

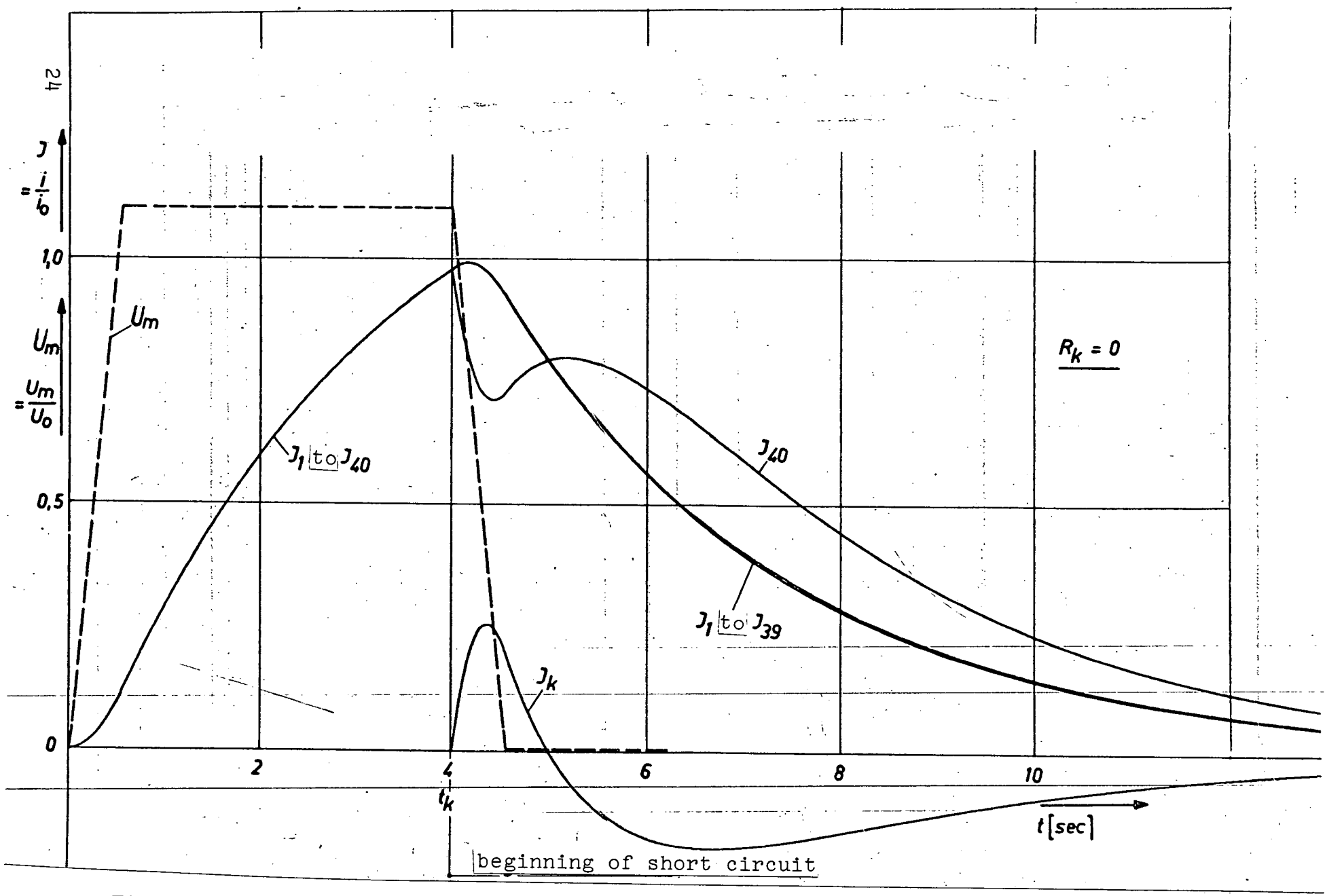

Figure 9. Coil currents $i_{(t)}$ and magnet voltage $u_{m(t)}$ for an ideal coil short circuit during the initial excitation phase with immediate generator de-excitation.

b) Coil short circuit during the flat-top phase with immediate initiation of generator de-excitation.

According to Figure 3, the flat-top phase extends between t_2 = 4.18 sec to t_3 = 14.18 sec. The time of the short circuit is then fixed at t_k = 5 sec.

/ 26

In addition, for this case we have

$$i_{(t)} = 40\ KA = I_N = const.$$
$$i'_{(t)} = 0$$

$$u_{m(t)} = \begin{cases} \text{corresponding to Eq. (6) for } t \leq t_k \\ u_{m2} - a(t - t_k) \quad \text{for } t_k \leq t \leq t_{k1} \\ 0 \quad \text{for } t_{k1} \leq t \leq t_E \end{cases}$$

$$R_k = 1\ m\Omega$$

The transient currents $i_{(t)}$ are shown in Figure 10.

c) Coil short circuit during the flat-top phase without generator de-excitation.

In this case the assumptions of b) apply. However, we will not introduce any premature de-excitation of the generator in this case, i.e. the pulse cycle of the undisturbed operation is maintained. The magnet voltage $u_{m(t)}$ follows the course given by equation (6), and it is shown together with the calculated transient currents in Figure 11.

The curves given in Figures 8 to 11 are given with a normalized representation using the following normalized values

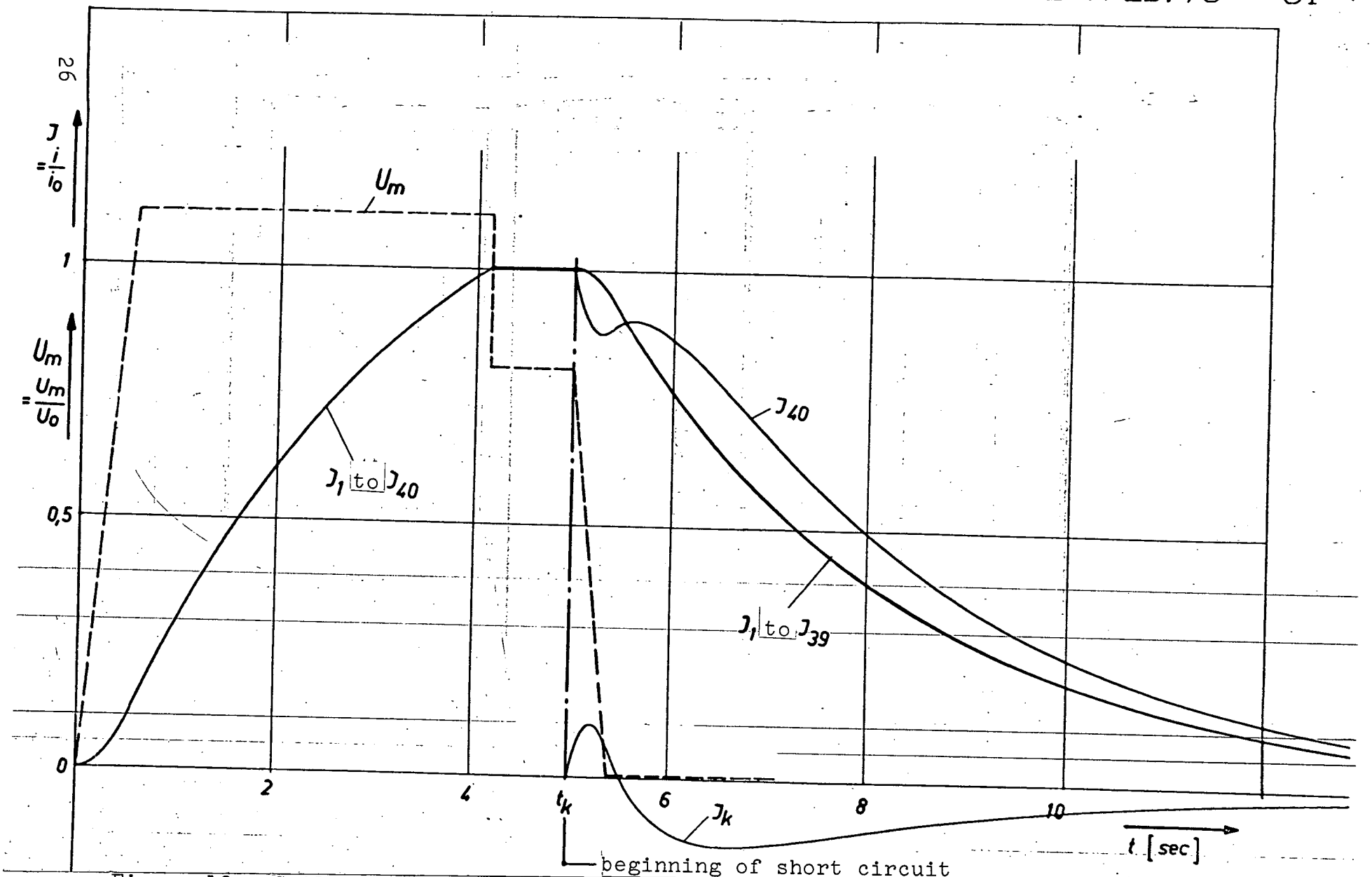

Figure 10. Coil currents $i_{(t)}$ and magnet voltage $u_{m(t)}$ for a coil short circuit during the flat-top phase with immediate generator de-excitation.

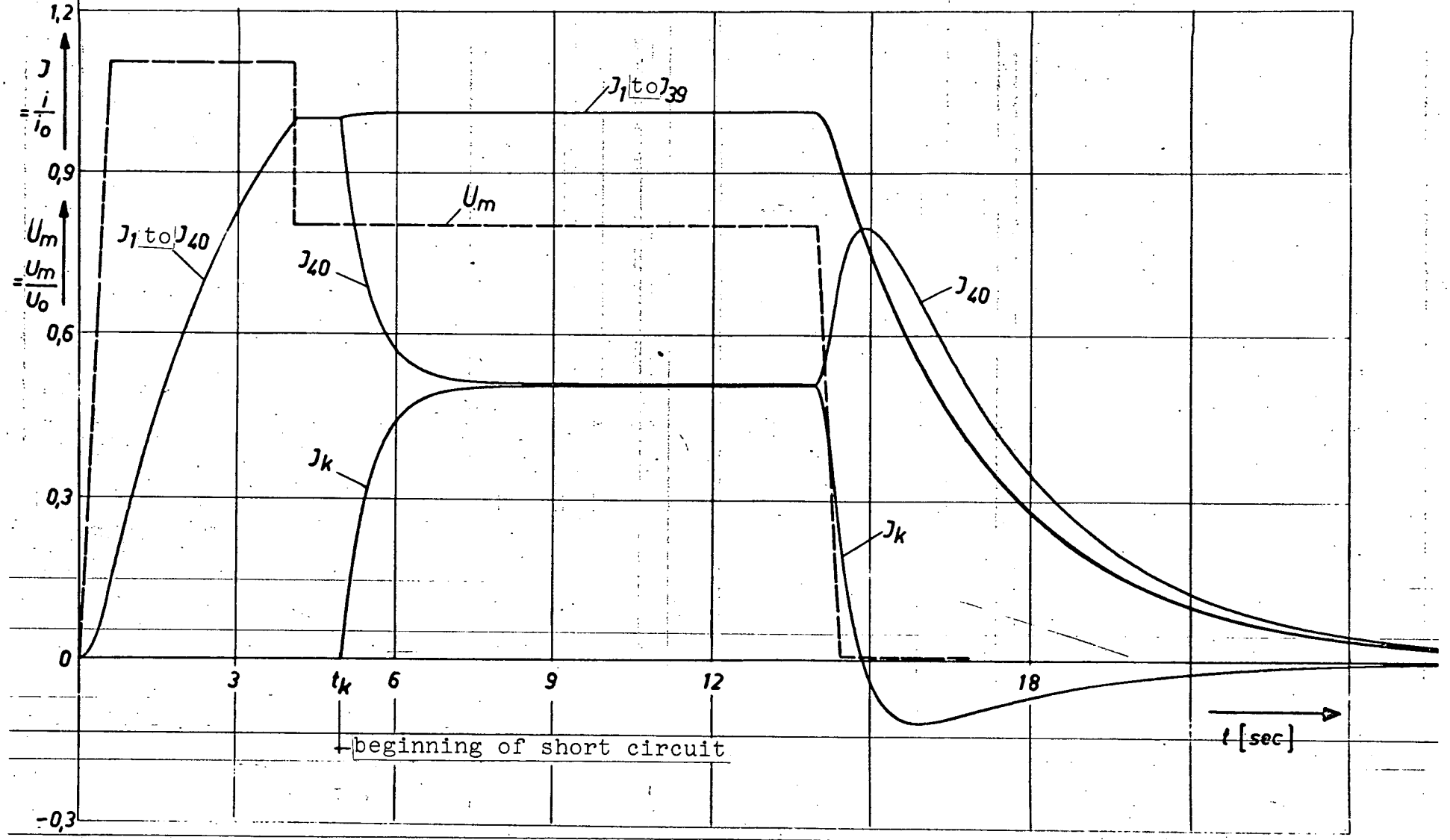

Figure 11. Coil currents $i_{(t)}$ and magnet voltage $u_{m(t)}$ for a coil short circuit during the flat-top phase without immediate generator de-excitation.

$$i_o = I_N = 40 \text{ KA}$$
$$u_o = 3 \text{ KV}$$

The notation and orientation follow from Figure 6. / 31

4.3 Numerical calculation of the magnetic forces

After the current intensities in the individual coils have become known from the beginning of a short circuit up to complete discharge of the magnet (Figures 8 to 11), we can now calculate the magnetic forces applied to the coil system as a function of time. The calculation will be done at certain points over the entire time range of an operational disturbance which starts at $t = t_k$. The Fortran routine "Kraefte" is used for this purpose. The routine is based on the magnetic force law (21) and is described in detail in [8].

The curves given in Figures 12 and 13 show the variation of the transient azimuthal and radial forces. The following correspondence holds

Case 4.2.a), Fig. 12 corresponds to Figure 8
Case 4.2.c), Fig. 13 corresponds to Figure 11.

Both diagrams only show the functions $K_{t1(t)} = K_{t39(t)}$ and $K_{r1(t)} = K_{r39(t)}$, because the largest forces are exerted on the coils N = 1 and N = 39 adjacent to the short-circuited coil N = 40. The change in direction of the forces $K_{t(t)}$ is remarkable (in Figure 5 they are shown with a positive direction). This occurs because during the discharge, we first have $i_{4o} < i_m$ and later on $i_{4o} > i_m$ (m=1 to 39). Also we can observe the change in the azimuthal forces $K_{t(t)}$ with the difference $\Delta i = i_N - i_{4o}$, ($i_N = i_{(t)}$ for N = 1 to 39), i.e. for $\Delta i = 0$ all $K_{t(t)} = 0$ and when

$\Delta i = (\Delta i)_{max}$ all $K_{t(t)} = K_{t(t)\,max}$. This is a general law, so that the forces $K_{t(t)}$ do not have to be calculated for a short circuit during the flat-top phase (Figure 10), because the current difference Δi under discussion is smaller over the entire time interval than the current difference after a short circuit during the initial excitation phase (Figure 8). In addition, the functions $K_{r(t)}$ of the radial forces drop off monotonically to zero after an operational disturbance is initiated, and therefore take on their maximum value during the undisturbed operation. /32

If there is not an immediate generator de-excitation, that is, the planned pulse cycle is maintained in spite of the short circuit, the currents $i_{(t)}$ first approach a new steady state (Figure 11). Over the steady range, we have Δi = const., which means that the functions $K_{r(t)}$ and $K_{t(t)}$ have a well-developed top range at the level of $K_{rstat} \approx 160$ Mp and $K_{tstat} \approx 120$ Mp respectively over a time interval of about 8 seconds (Figure 13). The subsequent de-excitation phase again has the characteristics of case 4.2.a).

Figure 14 shows the influence of the short circuit resistance R_k on the coil forces. The absolute magnitude of the resistance R_k of a short circuit can hardly be established because of the many ways in which it can be produced (connection of good or bad metallic conductors, arc transitions, etc.) It would be easy for the magnitudes of R_k to extend over several orders of magnitudes if we were to consider all the indicated possibilities. Therefore, it is certainly appropriate to determine the maximum forces K_{tmax} as a function of R_k. This is discussed for the short circuit case 4.2.a), which was found to be less favorable. The curve variation determined (Figure 14) shows that, even if an ideal short circuit R_k=0 is assumed, the maximum azimuthal

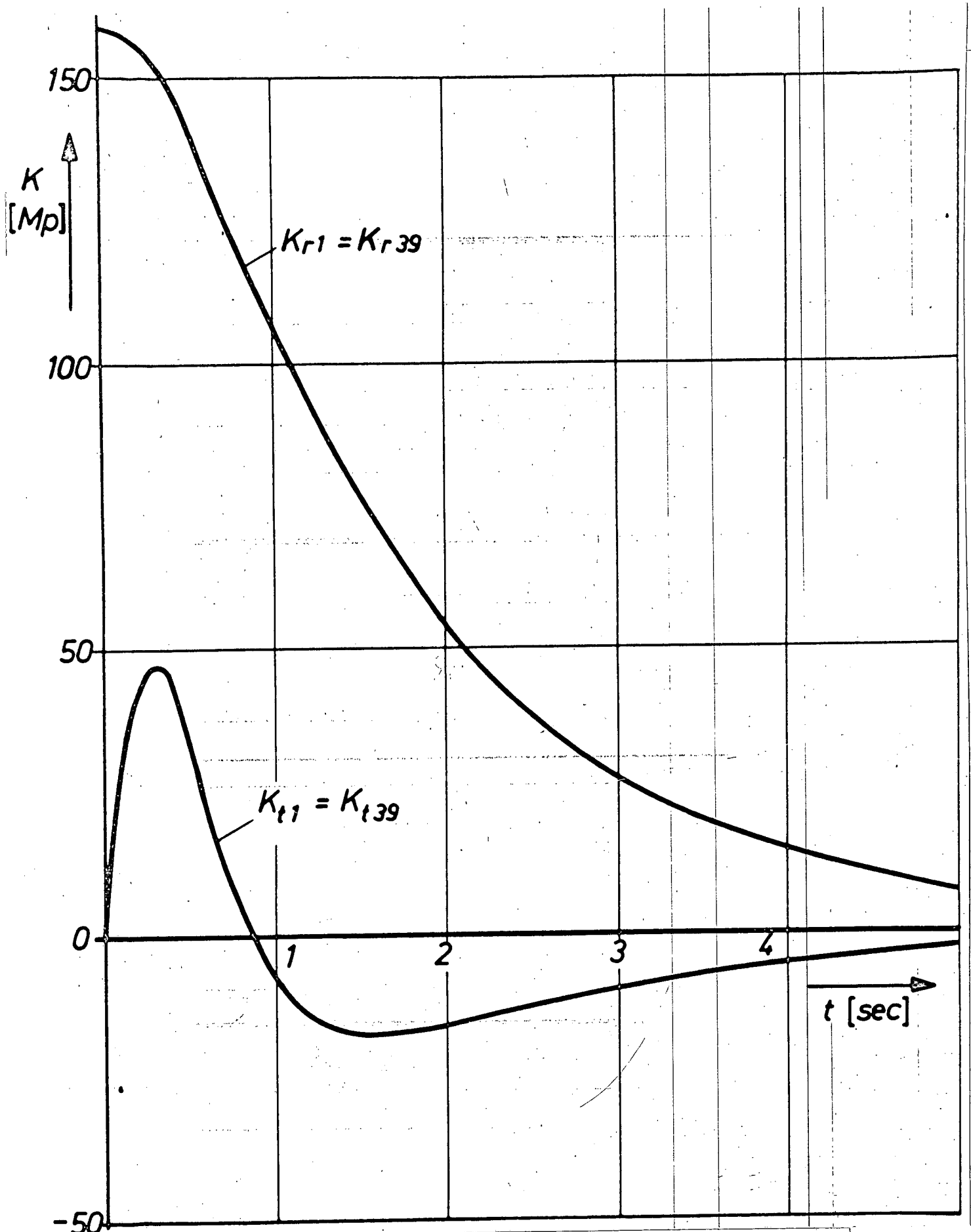

Figure 12. Azimuthal and radial forces applied to coils N=1 and N=39 which are adjacent to the short circuited coil N=40 after a short circuit in the initial excitation phase.

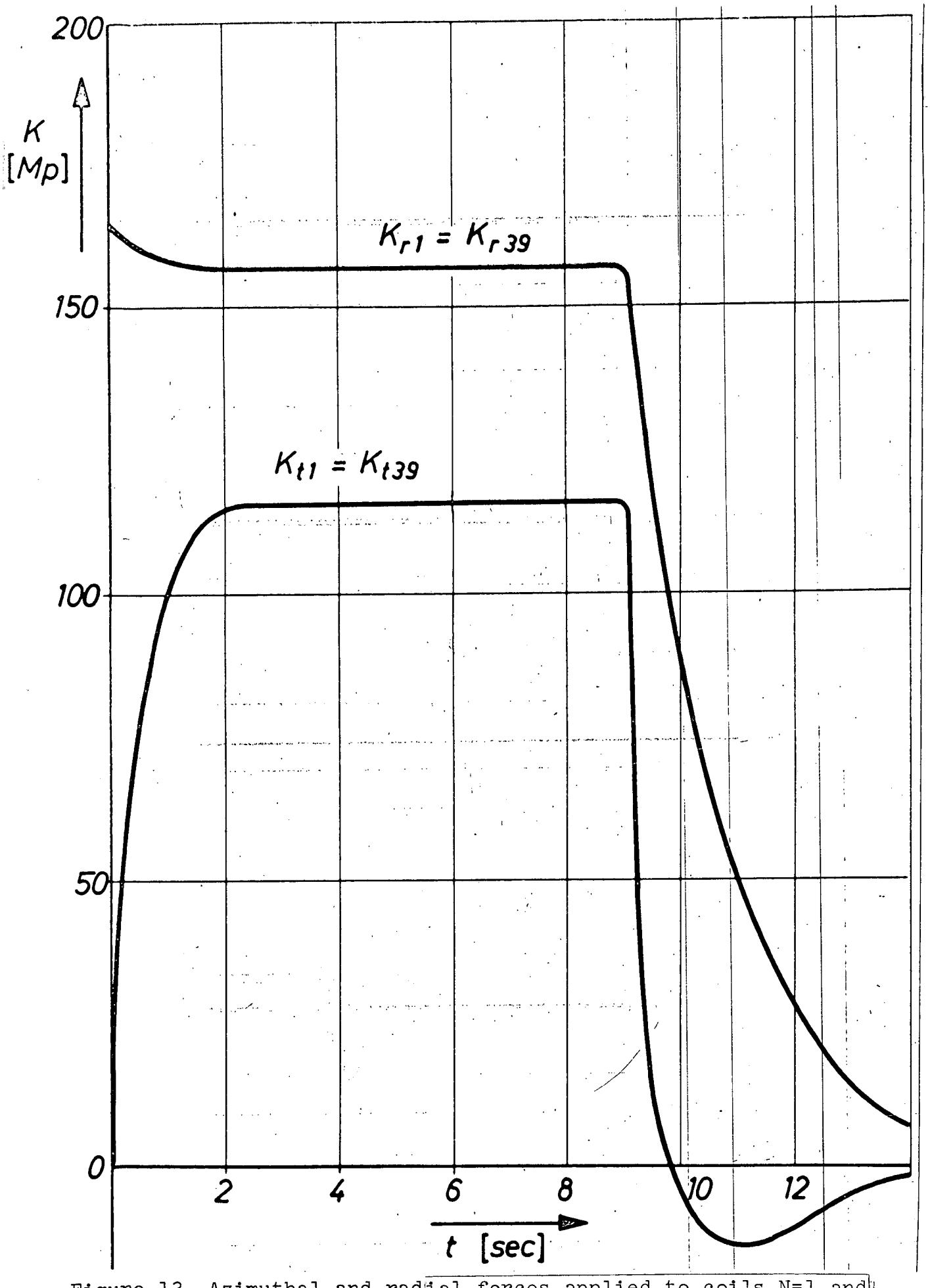

Figure 13. Azimuthal and radial forces applied to coils N=1 and N=39 adjacent to the short circuited coil N=40 after a short circuit during the flat-top phase without immediate generated de-excitation.

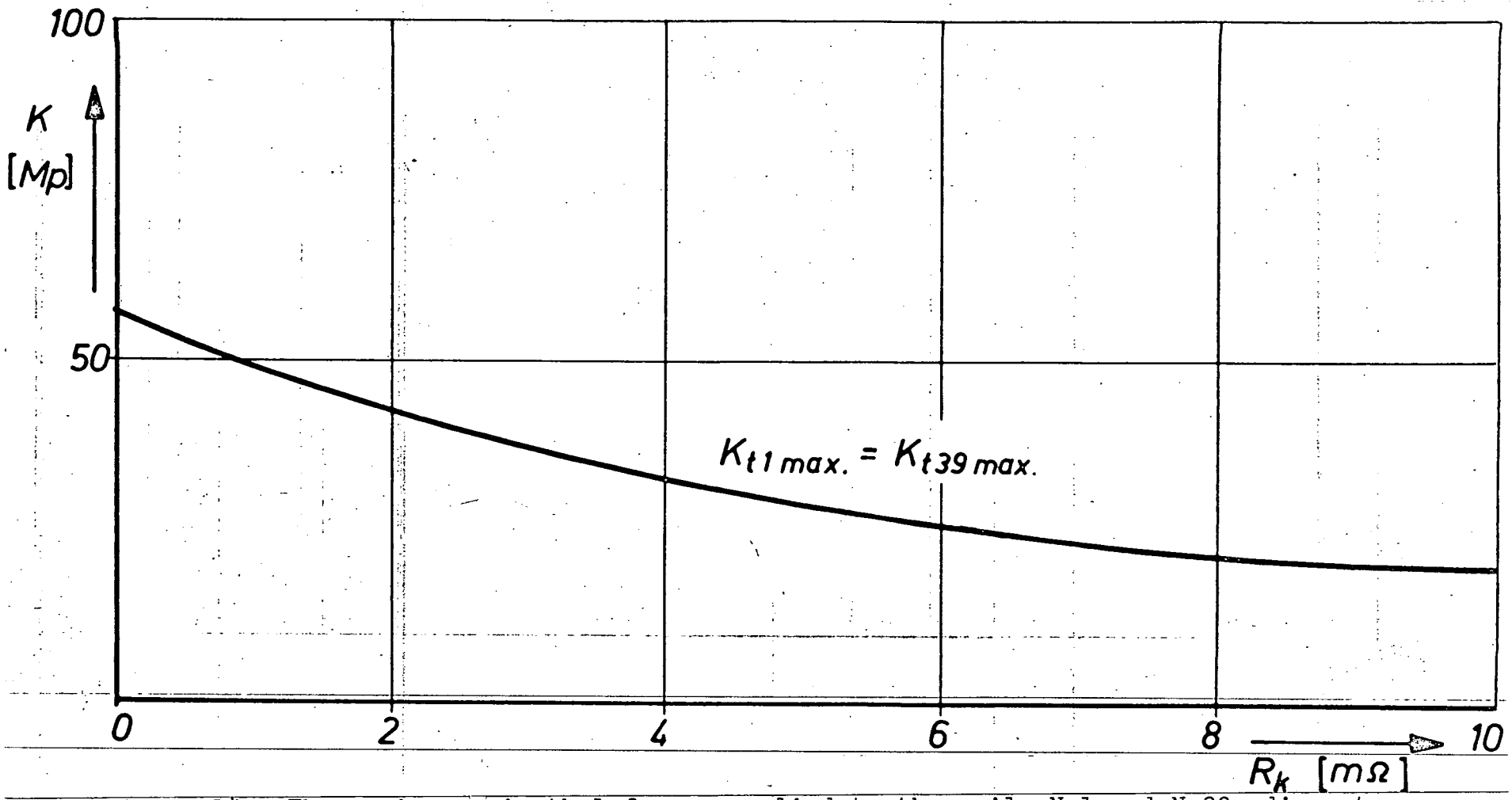

Figure 14. The maximum azimuthal forces applied to the coils N=1 and N=39 adjacent to the short circuited coil N=40 as a function of the short circuit resistance.

forces K_{tmax} = 60 Mp do not even approach the value of 291 Mp given in [1]. This means that the results presented here will have a positive influence on the construction of coils and the construction of the frame of the Stellarator.

/36

REFERENCES

1. Project Wendelstein W VII. IPP - Report 2/204, June, 1972.

2. Correction of Planning Data and Current Results for the Project Wendelstein W VII (Looseleaf book).

3. Equipment for High Energy Physics: CERN in Geneva Siemens Magazine,(Collection of papers from the Siemens Magazines, 2/71, 5/71, 6/71, 7/71 and 8/71).

4. Pöhlchen, R. Calculation of Self-Inductances of Thick Air-Core Coils, Mutual Inductances and Axial Forces between such Coils in Co-axial Systems by Means of a Digital Computer. Proc. Int. Conference on Magnet Technology, Hamburg 1970, pp. 142-151.

5. von Weiss, A. Introduction to Matrix Calculation for Applications in Electrical Technology. R. Oldenbourg-Verlag, München, 1971.

6. Preis, H. Analysis of Transient Processes in Linear Electrical Networks. IPP-Report 4/87, July, 1971.

7. Ralston, A. and H. S. Wilf. Mathematical Methods for Digital Computers, Volume I, Oldenbourg Verlag, 1967.

8. Pöhlchen, R. and Ch. Ludescher. Calculation of Net Forces and Mechanical Stress in the Toroidal Field Coil System of the Wendelstein VII, Pulsator and Wega, Proceedings of the VIIth Symposium on Fusion Technology, Grenoble, October, 1972.

9. Pöhlchen, R. and H. Preis. Calculation of Transient Currents and Forces in Toroidal Coil Systems for Fusion Machines. IPP-Report 4/107, January, 1973.

Translated for National Aeronautics and Space Administration under contract No. NASW 2483, by SCITRAN, P. O. Box 5456, Santa Barbara, California, 93108.